

A New Internal Mode in F-Actin Helps Explain the Remarkable Evolutionary Conservation of Actin's Sequence and Structure

Vitold E. Galkin, Margaret S. VanLoock, Albina Orlova, and Edward H. Egelman¹
Department of Biochemistry and Molecular Genetics
University of Virginia Health Sciences Center
Charlottesville, Virginia 22908

Summary

Actin is one of the most highly conserved eukaryotic proteins. There are no amino acid changes between the chicken and human skeletal muscle isoforms, and the most dissimilar actins still share more than 85% sequence identity [1]. We suggest that large discrete internal modes of freedom within the actin filament [2] may account for a significant component of this conservation, since each subunit must make multiple specific interactions with neighboring subunits. In support of this, we find that the same state of tilt of the actin subunit exists in both yeast and vertebrate striated muscle actin, and that in both the two domains undergo a “propeller rotation.” A similar movement of domains has also been seen in hexokinase [3, 4], Hsc70 [5], and Arp2/3 [6], all structural homologs of actin [7], suggesting that such an interdomain hinge motion is common to proteins in this superfamily [8]. Subunit-subunit interactions within the actin filament involve sequence insertions that are not present in MreB, a bacterial homolog of actin [9]. Remarkably, we find that in the tilted state actin subunits make new contacts with neighboring subunits that also involve these inserts, suggesting a key role for these elements in F-actin polymorphism.

Results and Discussion

In the presence of either human or plant actin depolymerizing factor (ADF), short segments of skeletal muscle actin filaments were found in which ADF was not regularly bound and in which the actin subunits had a tilt of $\sim 10^\circ$ – 12° from their position in normal F-actin [10]. It was proposed that these regions might be intermediates in filament disassembly. The visualization of such a local conformational change was entirely dependent upon the use of a new approach to image analysis of helical polymers, iterative helical real space reconstruction (IHRSR) [11], since the averaging of long filaments by traditional means [12] would obscure this transition that may only involve relatively short segments (~ 10 subunits). This method has also been shown to be quite powerful, by separating heterogeneous structures into homogeneous subsets, in applications with pure actin filaments [13] and complexes of F-actin with another actin binding protein [14]. To determine if the observed tilt of the subunits is introduced only by ADF proteins

in muscle actin, or if it is a more general property of all actins in complexes with ADF/cofilin-type molecules, we have now examined complexes of yeast F-actin with both yeast cofilin and human ADF (hADF) and a complex of muscle actin with hADF and have searched for regions in decorated filaments in which the actin was not regularly decorated. Figure 1 shows the application of the IHRSR method to both the undecorated yeast F-actin and muscle F-actin segments that have been found. The average “twist” of both muscle and yeast F-actin in the absence of other proteins is $\sim 166^\circ$ per subunit. The twist of the tilted muscle F-actin converges to $\sim 161^\circ$ per subunit in these naked patches, similar to the twist imposed by cofilin on extensively decorated filaments [10, 15]. In contrast, in the yeast filaments, the twist converges to $\sim 153^\circ$ per subunit, resulting in a distance between “crossovers” of the two long-pitch helical strands of ~ 190 Å (Figure 2G), as opposed to crossover distances with a mean of ~ 350 Å in pure yeast F-actin (with a mean twist of $\sim 166^\circ$) (Figure 2F). Despite the differences in twist, both the yeast and muscle reconstructions appear to be very similar to each other and very different from normal F-actin reconstructions (Figure 2A). Although no significant amounts of ADF or cofilin are seen in these reconstructions, we cannot differentiate between the possibility that these molecules are present but bound in a very disordered manner and the possibility that they are completely absent. A disordered mode of binding would mean that they would not be seen after averaging and the imposition of helical symmetry.

Earlier work had suggested that the subunits within these regions were tilted by $\sim 10^\circ$ – 12° from their normal position in F-actin [10]. Significant improvements in the reconstruction of muscle actin in this unusual state, as well as an entirely independent reconstruction of yeast F-actin in this conformation, have allowed us to see that, not only is the subunit tilted by $\sim 20^\circ$, but the two major domains must undergo the same type of “propeller rotation” (Figure 3C) in both muscle and yeast filaments to fit existing crystal structures of G-actin [16, 17] into these reconstructions (see Movie 1 in the Supplementary Material available with this article online). The axial rise per subunit remains at ~ 27 Å in these segments, despite the tilt of the subunit, the propeller rotation that occurs within the subunit, the large change in the overall twist of the filament (from $\sim 166^\circ$ to $\sim 153^\circ$ per subunit in yeast), and the new contacts that are made between adjacent subunits. This is consistent with reports showing that the axial rise per subunit in F-actin is quite invariant, with changes of less than 0.08 Å per subunit under conditions of maximal tension in muscle [18–20].

The magnitude of the propeller rotation, $\sim 30^\circ$ (Figure 3E), required to fit the actin crystal structure into the tilted reconstructions can be compared with what has previously been observed for this family of proteins. A relative rotation of the two major domains by $\sim 10^\circ$ was seen between two crystal structures of β -actin [16]. A new crystal structure for ADP- α -actin showed rotations

¹Correspondence: egelman@virginia.edu

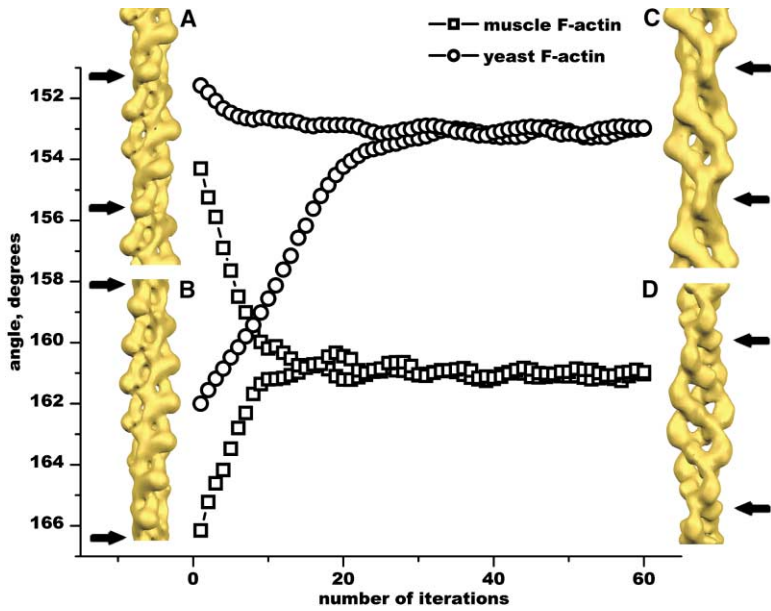


Figure 1. The IHRSR Method for Image Analysis

The IHRSR method [11] for image analysis of helical filaments is quite powerful for separating out discrete states of twist and structure within F-actin. Shown are two starting reference volumes (a and b), which are low-resolution versions of the Holmes model for F-actin [28], and resulting reconstructions for (c) yeast actin and (d) muscle actin. The (a) reference volume has been generated with a symmetry of 152° per subunit, while the (b) reference volume has a symmetry of 166° per subunit. This difference in twist leads to a large difference in the distance between crossovers of the right-handed long-pitch helical strands in F-actin, indicated by the arrows (a and b). The 503 segments of muscle actin, selected as being undecorated within filaments extensively decorated with hADF, were reconstructed with IHRSR, starting with the references having symmetries of either 166° or 154° . The open squares show the convergence of the symmetry to the value of 161° , and both paths resulted in the reconstruction shown in (d), even though the starting models

have very different symmetries and conformations from the result found. For the yeast actin, a similar procedure is shown (open circles), in which 1,240 segments have started IHRSR using the initial models with symmetries of 152° and 162° but converge to a symmetry of 153° after 60 cycles, with the resulting reconstruction shown in (c).

of subdomains 2 and 4 of $\sim 10^\circ$ and $\sim 5^\circ$, respectively, when compared with structures for ATP- α -actin [21]. Yeast hexokinase has a 12° rotation of the two major domains between the apo- and glucose-bound forms [3]. Crystal structures for different states of DnaK and Hsc70 do not exist, but solution small-angle X-ray scattering experiments have shown that there is a change in the radius of gyration of 1–2 Å for DnaK [22] and of 4–5 Å for Hsc70 [5] induced by binding ATP. The radius of gyration that we calculate for β -actin in the propeller-rotated state is only 0.6 Å greater than the radius of gyration of this molecule in the open crystal state [16], while the radius of gyration of the subunit in the open crystal state is 0.6 Å greater than the radius of gyration

of the molecule in the closed state [17]. Most significantly, an $\sim 30^\circ$ rotation of one of the major domains was required [8] to superimpose the nucleotide-bound structures of actin [23] or Hsc70 [24] onto the nucleotide-free hexokinase structure [25]. Perhaps the most important comparison is with the structures that have recently been determined for actin-related protein 2 (Arp2) and Arp3 [6]. In Arp3, the central cleft is opened about 12° with respect to actin. In Arp2, however, not only is the central cleft open about 18° with respect to actin, but there is a propeller rotation of the major domains that is very similar to what we observe in the tilted state. It was proposed that nucleotide binding to the Arps induces domain rotations that make them more closely

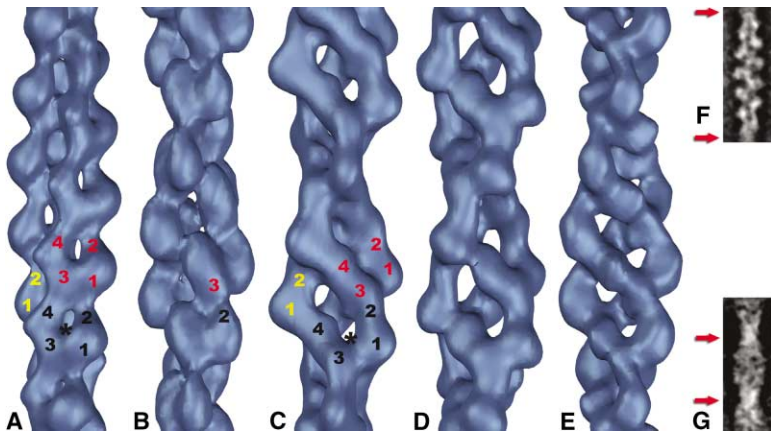


Figure 2. Three-Dimensional Reconstructions of Actin Filaments

(A) Reconstruction of normal yeast F-actin. (B) Reconstruction of a partially rotated state seen in disulfide-crosslinked F-actin. (C) Reconstruction of tilted yeast F-actin. (D) A low-resolution surface of an atomic model. (E) Reconstruction of tilted skeletal muscle F-actin.

Actin subdomains 1–4 have been labeled in (A)–(C), using different colors for different subunits. The (D) atomic model provides a very good match with both the (C) tilted yeast actin and the (E) tilted muscle actin. However, the twist of the tilted yeast and muscle actin is different, which can account for most of the differences between (C) and (E). For the (C) yeast actin, the twist is $\sim 153^\circ$ per subunit,

while for the (E) muscle actin, the twist is $\sim 161^\circ$ per subunit. The reduction of the angle between subunits to $\sim 153^\circ$ results in very short crossovers in these regions.

(F and G) In (G), a two-dimensional average of 144 segments from the set used for three-dimensional reconstruction (C) shows a crossover distance (red arrows) of ~ 190 Å. For comparison, the average crossover distance in normal yeast F-actin (A) is ~ 350 Å, and that can be seen in the average of 110 segments in (F).

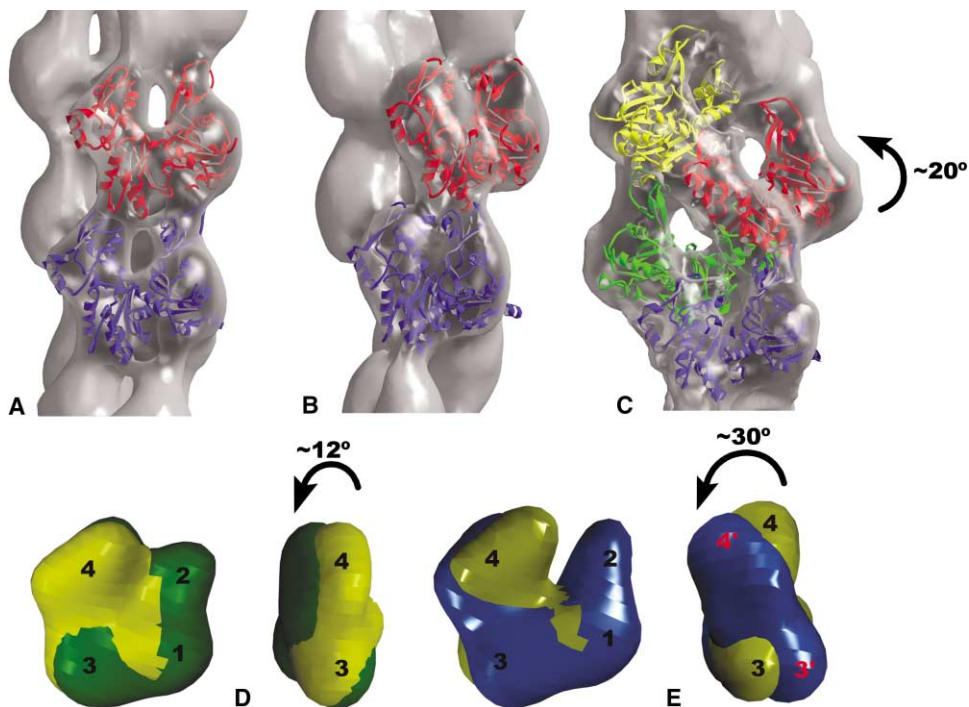


Figure 3. Models for Conformational Changes Associated with Tilting

- (A) Reconstruction of normal yeast F-actin.
 (B) Reconstruction of the partially tilted state of disulfide-crosslinked yeast F-actin.
 (C) Reconstruction of tilted yeast F-actin.

These reconstructions can be fit very well with atomic models. The molecular models used are: (A) unmodified X-ray crystal structure of β -actin with an open cleft [16], (B) a 12° propeller-rotated model of closed β -actin [17], and (C) a 30° propeller-rotated model of open β -actin [16].

(D) In this panel, the change in the actin subunit in (B) is shown.
 (E) In this panel, the change in the actin subunit in (C) is shown.

The crystal structures of the closed state of β -actin [17] ([D], yellow) and the open state of this molecule [16] ([E], yellow) have been modified by a 12° relative rotation of the two major domains ([D], green) or a 30° relative rotation of these domains ([E], blue) to fit the reconstructions in (B) and (C), respectively.

resemble nucleotide-bound actin and initiate nucleation of an actin filament [6]. An abundance of evidence suggests that large domain motions are a general property of this class of proteins.

To further probe the molecular details of this unusual state of F-actin, we have used the Q41C yeast actin mutant, which allows a disulfide to be formed between subdomain 2 (residue 41) of one actin subunit and subdomain 1 (residue 374) of an actin subunit above it on the same long-pitch helical strand [13, 26]. Under conditions of extensive crosslinking (~93% of all subunits are linked by a disulfide to an adjacent subunit), no segments of tilted actin were found after filaments were extensively decorated with yeast cofilin. However, ~1,000 segments were found (Figure 2B) that yielded a very stable reconstruction of a partially propeller-rotated state. We have been able to eliminate the possibility that this state is actually a mixture of segments that are tilted and rotated and segments that are untilted and unrotated by showing that segments cannot be sorted into two such classes using tilted and untilted references (data not shown). In normal F-actin, subdomain 2 makes a strong contact with subdomain 1 (Figure 2A), but in the tilted state of actin, subdomain 2 makes a strong contact with subdomain 3 (Figure 2C). In the crosslinked partially rotated state, subdomain 2 also appears to

make a contact with subdomain 3 (Figure 2B). This is surprising, since a covalent crosslink has been established between subdomain 2 and subdomain 1. Atomic modeling, however, shows that relatively small deformations of both the DNase I binding loop and the C terminus, two regions known to be flexible in actin [21, 23, 27], can allow the disulfide to exist in this different state (Figure 3B). In addition, the nucleotide binding cleft in the disulfide-bonded filaments is now closed (Figure 3B), which provides an additional means for the subunit to accommodate the strain imposed. Only finding this partially rotated state in the disulfide crosslinked filaments provides a very nice confirmation of the models proposed (Figure 3), since such a disulfide would be incompatible with the fully tilted state due to the large distance that now occurs between subdomain 2 and subdomain 1 above it.

The tilted state of actin clearly requires entirely new contacts to be made between subunits in the filament. An interesting question is how such contacts can switch in the filament without the filament breaking. One explanation may have to do with the fact that actin contains two “strands” of subunits, and a switching of contacts of one subunit would not break the filament as long as contacts are still made to this subunit by adjacent subunits on the opposite strand. Thus, it is possible that

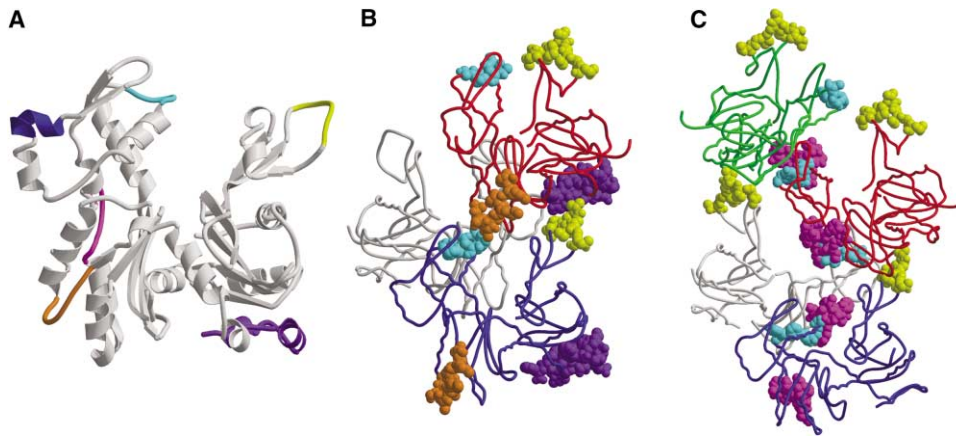


Figure 4. Sequence Inserts in Actin Not Present in Bacterial MreB

(A) The six sequence inserts that are present in all actins but absent in bacterial MreB [9] are shown in the G-actin structure. The color code is: yellow, residues 40–48 (DNase I binding loop, subdomain 2); cyan, residues 197–203 (subdomain 4); blue, residues 228–235 (subdomain 4); magenta, residues 262–274 (subdomains 3–4); orange, residues 319–327 (subdomain 3); and purple, residues 354–375 (subdomain 1). (B) The interactions between four of these inserts are shown in normal F-actin, in which the 40–48 insert (yellow) makes contact with the 354–375 insert (purple), and the 197–203 insert (cyan) makes contact with the 319–327 insert (orange). An interaction that is not shown involves the 262–274 insert making contact with the opposite strand. (C) In contrast, in tilted actin, the 262–274 insert (magenta) makes contact with the 197–203 insert (cyan), and the 40–48 insert (yellow) makes contact with subdomain 3 of an adjacent subunit.

such sequential switching could occur that would never break all contacts at the same time. It is also possible that the subunit does not rotate as a whole, and large internal deformations allow sequential switching within individual subunits. We suggest that the existence of such multiple contacts within F-actin provides strong additional constraints against mutation over a large surface of the actin subunit. The recent determination of a structure for the bacterial MreB protein showed that it is an actin homolog [9] and provides a framework for understanding the prokaryotic origin of actin-based motility, the cytoskeleton, and muscle. Interestingly, there are six sequence inserts that occur in all eukaryotic actins that are absent in MreB. Five of these appear to be involved in the subunit-subunit contacts that hold “normal” F-actin together (Figure 4A), with four of the five involved in contacts between inserts. Specifically, the DNase I binding loop in subdomain 2 (insert containing residues 40–48) is involved in contacts with the C-terminal insert (residues 354–375 of a subunit above it), and a loop in subdomain 4 (insert containing residues 197–203) is involved in contacts with a loop in subdomain 3 (insert containing residues 319–327) of a subunit above (Figure 4B). The fifth insert, residues 262–274, contains the “hydrophobic plug” that holds the two strands of F-actin together [28]. When the model of the tilted state is examined (Figure 4C), it is found that three of these six inserts appear to be involved in totally new contacts in the filament, with a loop on subdomain 4 (residues 197–203) now making a contact with the hydrophobic plug residues, 262–274, on an adjacent subunit. In contrast to the existing model of F-actin [28], in which this loop containing the hydrophobic plug must be swung out from its position in crystal structures of G-actin to make filament contacts, this loop makes reasonable contacts in the tilted state when it is in the G-actin crystal conformation (Figure 4C). The DNase I binding loop (insert containing residues 40–48), which

makes an important contact in normal F-actin with subdomain 1 of a subunit above it on the same long-pitch helical strand, now makes contact with subdomain 3 of the subunit above it (Figure 4C). This suggests that several of these sequence inserts play an extraordinary role in a number of different states of F-actin.

Over the course of eukaryotic evolution, virtually no differences have emerged in the structure of F-actin and only small differences have emerged in the sequence. Traditionally, the existence of large numbers of actin binding proteins was invoked to explain the selective pressure that might lead to such a conservation. However, the actin binding proteins themselves remain far less conserved, suggesting that this argument may be quite incomplete. Just as the ability of actin subunits to exist in states with large differences in twist has been shown to be a property of vertebrate α muscle [2, 10], vertebrate β -cytoplasmic (V.E.G. et al., unpublished data), and yeast actins [13], we now find that an unusual state of tilted, propeller-rotated actin subunits exists in both muscle and yeast actin filaments. We suggest that the ability of F-actin to support such internal modes may have been one of the most important conservative constraints. Since it has previously been shown that the crosslinking of subdomain 2 in actin to subdomain 1 of a subunit above it inhibits force generation by myosin, without interfering with actin’s activation of myosin’s ATPase [29], it is tempting to speculate that an internal mode such as the tilt we now observe may be important for actin’s interaction with myosin and other proteins.

Experimental Procedures

Sample Preparation and Electron Microscopy

Wild-type yeast actin, Q41C mutant actin, disulfide-crosslinked actin, and yeast cofilin were gifts from Dr. Emil Reisler’s laboratory. Human ADF was a gift from Dr. M.-F. Carlier.

All actin has been used as Mg^{2+} -F-actin in 50 mM KCl, 10 mM MOPS (pH 7.2), 2 mM $MgCl_2$. Wild-type or Q41C mutant yeast actin

(each at a concentration of 3 μ M) was applied (6–7 μ l) to lightly glow-discharged carbon-coated grids, then 2 drops (6–7 μ l each) of cofilin or hADF (each at a concentration of 8 μ M) were added for 2 min. Disulfide-crosslinked actin ([3 μ M]) was incubated with cofilin or hADF ([12 μ M]) for 10–12 min at room temperature, and 6 μ l of the mixture was applied to the grid. All samples were stained with 2% (w/v) uranyl acetate. Grids were examined in a Tecnai-12 (Philips) electron microscope under minimal dose conditions at an accelerating voltage of 80 keV and a nominal magnification of 30,000 \times .

Image Analysis

Yeast WT Actin

The SPIDER image processing Software [30] was used for most operations. Sorting of 14,610 segments against atomic models with different symmetries was as described [10]. A subset containing 1,042 segments selected by this sorting as having 167 $^\circ$ twist per subunit was then used for the reconstruction process. After 52 cycles of IHRSR, a symmetry of 167 $^\circ$ /27 \AA (rotation per subunit/axial rise per subunit) was found.

Yeast F-Actin Complexes with hADF or Yeast Cofilin, pH 7.2

A reconstruction of yeast F-actin (above) and previously published reconstructions of singly and doubly bound ADF-actin complexes [10] were used to create multiple references for the sorting of the raw images by both symmetry and the presence of additional mass. For this purpose, symmetries from 154 $^\circ$ to 176 $^\circ$, with a step size of 2 $^\circ$, were imposed on these volumes. Images showing the highest cross-correlation with the single ADF-occupied volume having a symmetry of 154 $^\circ$ –156 $^\circ$ were found to contain poorly decorated actin with a tilt of the subunits and a large conformational change within the subunit. The existence of a discrete state with this unusual twist and conformation was confirmed by the fact that three-dimensional reconstructions from these segments would always converge to the same structure, even if started with the Holmes model for F-actin [28] with very different symmetries as starting reference volumes.

Yeast Cofilin with S-S Yeast F-actin, pH 7.2

Filaments formed from the yeast Q41C mutant [26] were used under conditions in which 93% of the subunits were involved in at least one disulfide bond [10], and these filaments were incubated with yeast cofilin. A total of 14,735 filament segments were sorted by the presence of both additional mass and helical symmetry, as described above. Filament segments ($n = 1,360$) with the highest cross-correlation against the 154 $^\circ$ –156 $^\circ$ singly occupied references were used for IHRSR reconstruction. After 65 cycles, a symmetry of 157 $^\circ$ /27 \AA was found.

Q41C Mutant F-Actin, Noncrosslinked, with hADF, pH 7.2

A total of 10,750 segments were sorted by the presence of both additional mass and helical symmetry, as described above. The 154 $^\circ$ subset ($n = 344$) was used for IHRSR reconstruction, and after 155 cycles, a symmetry of 153 $^\circ$ /27 \AA was found. As a further test, the 154 $^\circ$ subsets from hADF/wild-type yeast F-actin and the yeast cofilin/wild-type yeast F-actin were combined together with these 344 segments and processed as described. After 80 cycles, 1,240 segments yielded a stable symmetry of 153 $^\circ$ /27 \AA . The resulting three-dimensional volume was indistinguishable from the one obtained with 344 segments.

Rabbit Muscle F-Actin with hADF, pH 7.8

Multireference alignment was used to sort 8,500 segments into three categories: naked actin, singly decorated actin, and doubly decorated actin. The 1,649 segments assigned to the naked actin group were first sorted by symmetry. A reference volume of the hADF singly decorated F-actin was used for sorting, employing a step size of 2 $^\circ$ in the symmetry. The 160 $^\circ$ –162 $^\circ$ subset ($n = 329$) was selected for IHRSR, and after 60 cycles yielded a stable solution with a 161 $^\circ$ /27 \AA symmetry. To confirm this result, an independent sorting was done based upon filament conformation. Reference volumes from hADF/Q41C F-actin (tilted, propeller-rotated state), pure wild-type yeast F-actin, and singly decorated hADF F-actin, all with a 162 $^\circ$ symmetry, were used for sorting. A subset of 503 images that corresponded to the tilted, propeller-rotated state was used for IHRSR. The final volume (161 $^\circ$ /27 \AA) was very similar to the one obtained by symmetry sorting.

Two-Dimensional Averages

Images of the wild-type yeast F-actin and of different ADF/cofilin-actin complexes were aligned against 90 reference projections, and

segments corresponding to projections with crossovers in the center were used for the reference-free alignment (AP SR within SPIDER).

Model Building

Crystal structures for both the closed- [17] and open-cleft [16] conformations of β -actin were used to generate low-resolution surfaces. Using shape as our primary guide, these surfaces were docked into the EM reconstructions. Transformations used in docking the surfaces were then applied to the atomic structure coordinates, followed by the imposition of helical symmetry to generate filament models. Models for the propeller-rotated actin were generated using the X-ray crystal structures of the actin subunit to first position subdomains 1 and 2 (outer domain) into the EM reconstructions. A rigid body rotation was then made about the bond between residues 147 and 148 until a best fit of the inner domain (subdomains 3 and 4) to the EM reconstruction was achieved.

Supplementary Material

Supplementary Material including two movies that show the changes that occur within the actin subunit (Movie 1) and in the subunit-subunit contacts (Movie 2) when actin undergoes the transition to the tilted state is available at <http://images.cellpress.com/supmat/supmatin.htm>.

Acknowledgments

We thank Drs. Emil Reisler and Alexander Shvetsov for the generous gift of yeast cofilin and the various yeast actins and Dr. Marie-France Carlier for the hADF. This work was supported by a National Institutes of Health grant to E.H.E.

Received: January 7, 2002

Revised: February 1, 2002

Accepted: February 1, 2002

Published: April 2, 2002

References

1. Sheterline, P., Clayton, J., and Sparrow, J. (1995). Actin. *Protein Profile* 2, 1–103.
2. Egelman, E.H., Francis, N., and DeRosier, D.J. (1982). F-actin is a helix with a random variable twist. *Nature* 298, 131–135.
3. Bennett, W.S., Jr., and Steitz, T.A. (1978). Glucose-induced conformational change in yeast hexokinase. *Proc. Natl. Acad. Sci. USA* 75, 4848–4852.
4. McDonald, R.C., Steitz, T.A., and Engelman, D.M. (1979). Yeast hexokinase in solution exhibits a large conformational change upon binding glucose or glucose 6-phosphate. *Biochemistry* 18, 338–342.
5. Wilbanks, S.M., Chen, L., Tsuruta, H., Hodgson, K.O., and McKay, D.B. (1995). Solution small-angle X-ray scattering study of the molecular chaperone Hsc70 and its subfragments. *Biochemistry* 34, 12095–12106.
6. Robinson, R.C., Turbedsky, K., Kaiser, D.A., Marchand, J.B., Higgs, H.N., Choe, S., and Pollard, T.D. (2001). Crystal structure of Arp2/3 complex. *Science* 294, 1679–1684.
7. Flaherty, K.M., McKay, D.B., Kabsch, W., and Holmes, K.C. (1991). Similarity of the three-dimensional structures of actin and the ATPase fragment of a 70-kDa heat shock cognate protein. *Proc. Natl. Acad. Sci. USA* 88, 5041–5045.
8. Bork, P., Sander, C., and Valencia, A. (1992). An ATPase domain common to prokaryotic cell cycle proteins, sugar kinases, actin, and hsp70 heat shock proteins. *Proc. Natl. Acad. Sci. USA* 89, 7290–7294.
9. van den Ent, F., Amos, L.A., and Lowe, J. (2001). Prokaryotic origin of the actin cytoskeleton. *Nature* 413, 39–44.
10. Galkin, V.E., Orlova, A., Lukyanova, N., Wriggers, W., and Egelman, E.H. (2001). Actin depolymerizing factor stabilizes an existing state of F-actin and can change the tilt of F-actin subunits. *J. Cell Biol.* 153, 75–86.
11. Egelman, E.H. (2000). A robust algorithm for the reconstruction

- of helical filaments using single-particle methods. *Ultramicroscopy* 85, 225–234.
12. DeRosier, D.J., and Klug, A. (1968). Reconstruction of three-dimensional structures from electron micrographs. *Nature* 217, 130–134.
 13. Orlova, A., Galkin, V.E., VanLoock, M.S., Kim, E., Shvetsov, A., Reisler, E., and Egelman, E.H. (2001). Probing the structure of f-actin: cross-links constrain atomic models and modify actin dynamics. *J. Mol. Biol.* 312, 95–106.
 14. Lukoyanova, N., VanLoock, M.S., Orlova, A., Galkin, V.E., Wang, K., and Egelman, E.H. (2002). Each actin subunit has three nebulin-binding sites: implications for steric blocking. *Curr. Biol.* 12, 383–388.
 15. McGough, A., Pope, B., Chiu, W., and Weeds, A. (1997). Cofilin changes the twist of F-actin: implications for actin filament dynamics and cellular function. *J. Cell Biol.* 138, 771–781.
 16. Chik, J.K., Lindberg, U., and Schutt, C.E. (1996). The structure of an open state of β -actin at 2.65 Ångstrom resolution. *J. Mol. Biol.* 263, 607–623.
 17. Schutt, C.E., Myslik, J.C., Rozycki, M.D., Goonesekere, N.C.W., and Lindberg, U. (1993). The structure of crystalline profilin: β -actin. *Nature* 365, 810–816.
 18. Kojima, H., Ishijima, A., and Yanagida, T. (1994). Direct measurement of stiffness of single actin filaments with and without tropomyosin using *in vitro* nano-manipulation. *Proc. Natl. Acad. Sci. USA* 91, 12962–12966.
 19. Wakabayashi, K., Sugimoto, Y., Tanaka, H., Ueno, Y., Takezawa, Y., and Amemiya, Y. (1994). X-ray diffraction evidence for the extensibility of actin and myosin filaments during muscle contraction. *Biophys. J.* 67, 2422–2435.
 20. Huxley, H.E., Stewart, A., Sosa, H., and Irving, T. (1994). X-ray diffraction measurements of the extensibility of actin and myosin filaments in contracting muscle. *Biophys. J.* 67, 2411–2421.
 21. Otterbein, L.R., Graceffa, P., and Dominguez, R. (2001). The crystal structure of uncomplexed actin in the ADP state. *Science* 293, 708–711.
 22. Shi, L., Kataoka, M., and Fink, A.L. (1996). Conformational characterization of DnaK and its complexes by small-angle X-ray scattering. *Biochemistry* 35, 3297–3308.
 23. Kabsch, W., Mannherz, H.G., Suck, D., Pai, E.F., and Holmes, K.C. (1990). Atomic structure of the actin:DNase I complex. *Nature* 347, 37–44.
 24. Flaherty, K.M., DeLuca-Flaherty, C., and McKay, D.B. (1990). Three-dimensional structure of the ATPase fragment of a 70K heat-shock cognate protein. *Nature* 346, 623–628.
 25. Anderson, C.M., Stenkamp, R.E., and Steitz, T.A. (1978). Sequencing a protein by x-ray crystallography. II. Refinement of yeast hexokinase B co-ordinates and sequence at 2.1 Å resolution. *J. Mol. Biol.* 123, 15–33.
 26. Kim, E., Wriggers, W., Phillips, M., Kokabi, K., Rubenstein, P.A., and Reisler, E. (2000). Cross-linking constraints on F-actin structure. *J. Mol. Biol.* 299, 421–429.
 27. Orlova, A., and Egelman, E.H. (1995). Structural dynamics of F-actin. I. Changes in the C-terminus. *J. Mol. Biol.* 245, 582–597.
 28. Holmes, K.C., Popp, D., Gebhard, W., and Kabsch, W. (1990). Atomic model of the actin filament. *Nature* 347, 44–49.
 29. Kim, E., Bobkova, E., Miller, C.J., Orlova, A., Hegyi, G., Egelman, E.H., Muhrad, A., and Reisler, E. (1998). Intrastrand cross-linked actin between Gln-41 and Cys-374. III. Inhibition of motion and force generation with myosin. *Biochemistry* 37, 17801–17809.
 30. Frank, J., Radermacher, M., Penczek, P., Zhu, J., Li, Y., Ladjadj, M., and Leith, A. (1996). SPIDER and WEB: processing and visualization of images in 3D electron microscopy and related fields. *J. Struct. Biol.* 116, 190–199.